The role of lamination conditions on the electrochemical behaviour of NMC811/graphite cells

Journal of Energy Storage 137 (2025) 118584

Contents lists available at ScienceDirect

Journal of Energy Storage

journal homepage: www.elsevier.com/locate/est

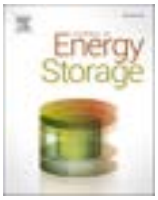

Research papers

The role of lamination conditions on the electrochemical behaviour of NMC811/graphite cells

Daniele Versaci [a,*], Silvio Fugattini [b], Michele Serri [b], Andrea Moselli [b], Julia Amici [a], Silvia Bodoardo [a]

[a] Politecnico di Torino, Department of Applied Science and Technology, Electrochemistry Group, Corso Duca Degli Abruzzi, 24, 10129, Torino, Italy
[b] Manz Italy srl, Via S. Lorenzo 19, 40037, Sasso Marconi, Bologna, Italy

ARTICLE INFO

Keywords:
Lithium-ion battery
Lamination
NMC811
Cell manufacturing
Separator
MacMullin
Gurley number

ABSTRACT

The lamination process between electrodes and separator is a crucial step in manufacturing lithium-ion cells, with a direct impact on production yield and electrochemical performance. In this study, a systematic analysis of the effect of two lamination parameters, temperature and pressure, on NMC811/graphite full cells was conducted. The impact of the lamination process on the separator properties was evaluated through permeability test, ionic conductivity, and morphological analyses. The results showed a dual effect: modification of the porous structure of the separator, as a function of the lamination conditions, with variations in the permeability and ionic conductivity of the system. At the full cell level, the most extreme lamination conditions led to a higher initial Coulombic efficiency, better wettability, lower data dispersion and a significant reduction in internal resistance. Furthermore, better performance at high C-rates and a higher capacity retention after 100 cycles were observed. This study confirms that a systematic optimization of the lamination can improve the electrochemical stability and reliability of the cells, depending on the materials chosen, and potentially reduce production scrap.

1. Introduction

Rechargeable lithium-ion batteries (LIBs) have dominated the battery market for several years. Since their introduction in the early 1990s, they have undergone continuous and progressive evolution, allowing them to replace other rechargeable battery technologies. Nowadays, LIBs power a vast range of devices: from small everyday devices to medical equipment, electric bikes, drones, cars, and other transportation systems. The progressive improvement that LIBs have shown in just over 30 years makes them one of the leading players in the ongoing green energy transition [1,2].

In recent decades, research has predominantly focused on studying and improving cell components, such as active materials, binders, electrolytes, current collectors, and separators [3–11]. Conversely, less attention has been focused, at the academic level, on the analysis and optimization of the lithium-ion cell manufacturing process, which remains a complex system comprising a series of interconnected and sequential steps [12–16].

Three key aspects must be considered in the production of lithium-ion cells: performance, sustainability, and cost [17]. While these factors are certainly influenced by the choice of materials, as previously mentioned, the various steps of the manufacturing process also play a fundamental role [12]. For example, with the increasing number of new gigafactories, with new and innovative production lines, scrap rates are inevitably increasing [18]. Recent studies indicate that scrap generation during battery manufacturing remains significantly high, exceeding the expected target of less than 10 % of total scrap [19]. Considering that manufacturing accounts for approximately 25 % of the total cost of LIBs, optimizing each step of the manufacturing process can potentially enhance performance, improve sustainability, and simultaneously reduce costs [13].

In particular, among the various steps of the production process, stacking is one of the bottlenecks in terms of productivity, since it is a time-consuming process [13,20]. During the stacking process, particular attention must be paid to prevent damage to the electrodes and separator, as well as to avoid cross-contamination and misalignment issues, which can easily result in scrap or cell failure [21–24]. To address the limitations of traditional stacking processes, higher-productivity continuous stacking methods have been studied and implemented, offering significant improvements in process speed. Among the alternative

* Corresponding author.
E-mail address: daniele.versaci@polito.it (D. Versaci).

https://doi.org/10.1016/j.est.2025.118584
Received 14 May 2025; Received in revised form 4 August 2025; Accepted 24 September 2025

stacking processes, the lamination process of electrodes with the separator is widely employed on an industrial scale for the production of lithium-ion cells [20]. The primary objective of lamination is to physically bind the electrodes (anode and cathode) to the separator, thereby simplifying the stacking process while significantly reducing defects arising from misalignment in the anode-separator-cathode stack. Thus, this procedure ensures a physical connection between the interlayers, separator/cathode and separator/anode, maximizing contact between the electrodes/separator surfaces and minimizing discontinuities at the interfaces. More in detail, the physical adhesion between electrodes and separator is achieved through the thermal softening of a binder layer (*e.g.*, PVDF), typically added on the surface of the separator for this purpose, combined with the application of a force to the anode/separator/cathode stack or a heating process *via* the lamination roll system [20].

Typically, the optimized lamination process offers several production line advantages, such as simplification and automation of the stacking process, increased production line speed, and reduced scrap rates caused by electrode-separator misalignment. However, recent studies have shown that the lamination process and its optimization can also influence the performance and reliability of lithium-ion cells [20,25–28]. For example, the studies carried out by Frankenberger et al. revealed that lamination of the anode-separator interface significantly reduces the continuous and uncontrolled growth of the solid-electrolyte interphase (SEI), with significant improvement in terms of capacity retention and cyclability [27]. Meanwhile, the lamination at the cathode-separator interface improves the initial contact between materials, reducing the initial surface resistance. Other studies have shown a correlation between lamination and the electrolyte permeability in the electrode-separator stacks, highlighting how the lamination process can enhance the wettability of the samples [25]. In general, these studies have shown that any variations in the lamination process, and consequently the adjustments of its governing parameters, can significantly impact the electrochemical performance of the final LIB cell, particularly in terms of long-term cyclability and stability at high C-rates [28].

In the present study, two lamination parameters (roll applied pressure and temperature) were evaluated, and their impact on the final electrochemical performance of NMC 811/graphite full cell was evaluated. Particular attention was paid to the impact of the lamination process on the separator properties, and how this affects the electrochemical behaviour. The study was conducted by systematically varying the parameters of the lamination process, applied directly to a complete anode-separator-cathode stack. This approach enables the evaluation of the lamination process in its entirety, simulating real-process conditions where both electrodes are simultaneously aligned and bond to the separator. This aspect is particularly relevant, as, to the best of our knowledge, only few academic studies systematically examine the impact of the lamination process under full-stack conditions and in real-application scenarios, evaluating the impact on the final battery performances.

2. Materials and methods

2.1. Lamination process

For the present study, commercial single-side coated electrode sheets (NEI Corp., USA) were selected. NMC 811 was chosen as the cathode (Slurry formulation: 90:5:5 Active material:SuperP:PVDF, Active Material Loading: 10.0 mg cm^{-2} ± 5 %, Standard Areal Capacity: 2.0 mAh cm^{-2} ± 5 %), while a natural graphite-based electrode (Slurry formulation: 90:5:5 Active material:SuperP:PVDF, Active Material Loading: 6.5 mg cm^{-2} ± 5 %, Standard Areal Capacity: 2.4 mAh cm^{-2} ± 5 %) was chosen as the anode.

For the lamination process, 3 × 3 cm (area = 9 cm^2) cathode and 3.5 × 3.5 (area = 12.25 cm^2) anode electrodes were obtained from the commercial sheets, with a final N/P ratio of 1.2. While a polyolefin-based trilayer separator (PP/PE/PP) with a PVDF coating (Celgard R0542C) with a total thickness of 20 μm was used.

Cathode, anode, and separator were laminated to make a single stack by using a lamination machine (LH200, Manz Italy), able to vary the feeding speed, linear pressure, and temperature by pre-heating modules. Fig. S1 shows a technical diagram of the pre-industrial lamination machine.

All laminated samples were subjected to HI-POT measurements (IR3455, Hioki), applying to the stack a high-voltage stress of 500 V for 1 s to identify the effective electrical insulation of the separator and exclude the risk of cell short circuits due to excessive stretching of the separator during the lamination process or to the presence of electrode edge defects.

2.2. Separator characterization

The laminated separators were subjected to air permeability tests. Air permeability was used to estimate the Gurley number, defined as the time required for the air to pass through a defined region of the separator, under particular pressure. Before the measurement, the samples were immersed in an isopropanol bath for 30 min, in order to promote the chemical peel-off of the electrodes from the separator. Afterward, the separator was dried in air for 30 min, before the Gurley number estimation test. Air permeability measurements were performed using a Gurley Densometers testers (4340, GPI). For each sample, the analysis was conducted on multiple separators and in three different areas to ensure the accuracy and consistency of the measurement.

After the Gurley number measurement, the separators were cut into 18 cm disks and further dried at 60 °C under vacuum for 12 h (Büchi Glass Oven B-585) to ensure complete removal of solvent and trapped air from the pores. Subsequently, the separator disks were immersed in the electrolyte for 48 h inside a glovebox (MBraun Labstar, H_2O and O_2 content < 1 ppm). Finally, separators consisting of one to four layers were sandwiched between two stainless steel electrodes in an ECC-Std electrochemical test cell (EL-CELL GmbH). The cell was placed in a climate chamber (MKF 56, Binder) at a controlled temperature of 25 °C and subjected to repeated electrochemical impedance spectroscopy (EIS) analyses. Impedance measurements were carried out in the frequency range of 500 kHz to 50 mHz with an AC amplitude of 10 mV, using a VMP3 potentiostat (Biologic). Before each EIS measurement, the cell was allowed to rest and stabilize for 45 min. The average resistance of the different separator stack was determined from multiple measurements. The bulk resistance (R_{ion}) of the electrolyte-soaked separators was determined from the high-frequency intercept of the impedance spectra, by an equivalent circuit fitting, consisting of a serial connection of an inductor I, a resistor R, and a constant phase element CPE. The ionic conductivity in the separator soaked with the electrolyte (σ_{Sep}) was then calculated using the equation:

$$\sigma_{Sep} = \frac{l}{A} \cdot \frac{1}{R_{ion}/N} \quad (1)$$

where l is the thickness of the separator membrane (20 μm), A is the area of the stainless-steel blocking electrodes (2.54 cm^2), and N is the number of separator layers.

The MacMullin numbers (N_m) were obtained by dividing the conductivity of the pure electrolyte (σ_{EL}) by the conductivity of the separator filled with electrolyte (σ_{Sep}):

$$N_m = \frac{\sigma_{el}}{\sigma_{sep}} \quad (2)$$

The ionic conductivity of the pure electrolyte was measured in a climate chamber (MKF 56, binder) at 25 °C using a Amel 192 K1, Pt electrodes, K = 1.

A morphological analysis of the delaminated separators was conducted using Field emission scanning electron microscopy analysis (FESEM, Zeiss SUPRA TM 40 with Gemini column and Schottky field

emission tip). Multiple areas of each sample were examined at different magnifications to assess the effects of the lamination process (acceleration voltage of 5 kV and working distance within 2.1–8.5 mm, with magnification up to 150 kX). Additionally, for separators laminated between two electrodes (anode and cathode), both sides were analysed to distinguish the individual contributions of each electrode to the separator morphology after lamination.

2.3. Cell assembling and electrochemical characterization

For the electrochemical test, after the lamination process, nickel and aluminum tables (4 mm width, MTI) were bonded with the electrodes using battery-grade strapping tape (High-Temperature Insulation Strapping Tape in PET, 0.03 mm thickness). The pre-assembled stacks were dried at 60 °C for 12 h under vacuum (Büchi Glass Oven B-585), then transferred in a dry room (dew point −26 °C) for full-cell assembly. The stacks were inserted in a laminate-type aluminum pouch film (thickness of 0.115 mm, MTI) used as pouch cell case, filled with 1.5 mL electrolyte and sealed under vacuum. For all the electrochemical tests, the electrolyte was a solution of 1 M $LiPF_6$ in ethylene carbonate (EC): ethyl methyl carbonate (EMC) 3:7 v/v (LP57, Elyte).

Before starting the forming cycles, the cells were rested at OCV for 24 h to monitor the internal resistance by EIS, and to guarantee the electrolyte permeability inside the electrode and the separator. The as-prepared pouch cells were cycled at RT (25 ± 2 °C) between 3 V and 4.15 V, using a CCCV protocol (constant current followed by constant voltage protocol) for charging, and CC protocol for discharging.

3. Results and discussion

The optimal lamination parameters were defined through preliminary tests by the lamination of two aluminum sheets with the separator and systematically varying linear pressure and temperature, keeping the feeding rate fixed, as reported in Table 1. The feed rate was set to 100 mm s^{-1} to simulate a process closer to the industrial one.

This pre-screening analysis permits the identification of the most significant lamination conditions while excluding those that are either too extreme, leading to separator damage, or too soft and ineffective. For this study, aluminum sheets were chosen, as they are commonly used as current collectors in the cathode electrodes of LiBs. Their smooth surface facilitates a more accurate evaluation of the combined effects of lamination temperature and pressure, minimizing the potential interference from surface irregularities. It is worth noting that aluminum foils were intentionally employed to explore boundary conditions in which the separator may experience permanent deformation or failure even in the absence of active material on the current collector. This approach enabled us to isolate and assess the direct influence of lamination conditions on the separator, independently of other electrode-related variables.

Two types of analyses were carried out to assess the impact of the lamination process on the separator properties: the measurement of the Gurley and MacMullin numbers. For each set of lamination conditions, two separator samples were analysed. The measurements were taken from three different areas on each separator, with five repetitions per area, to ensure a robust statistical data distribution. The descriptive statistical analysis results are reported in Table 2.

The qualitative understanding of the porosity of the separator can be obtained by measuring the gas permeability, in terms of Gurley number. The Gurley number is expressed in seconds and represents the time required for 100 cm^3 air to pass through a separator under a specific pressure (ASTM D726) [29]. Typically, a lower Gurley number corresponds to higher porosity and lower tortuosity [30–32]. It is important to note that, in our case, the Gurley number measured for the pristine sample is higher than the value reported by the manufacturer. This discrepancy may result from the fact that the pristine separator was immersed in an isopropanol bath and subsequently dried before the measurement, to allow a direct comparison with the delaminated separators. Therefore, the Gurley number analysis provides a relative measure, as the primary goal is to better understand how the lamination conditions affect the separator permeability compared to the pristine sample. Table 1 shows that all the investigated lamination processes on Al/separator/Al stacks lead to an increase in the Gurley number, indicating lower permeability and, consequently, a reduction in porosity, as expected [31,33]. Except for condition A, which shows a higher Gurley value than conditions B and C, an increasing trend of the Gurley number is observed as the lamination conditions become progressively more stressful.

To evaluate the reliability and consistency of the data collected in the three different areas of each separator, a statistical analysis was performed. The box chart (Fig. 1) illustrates the distribution of the data collected for each lamination condition across the three areas of the separator.

Different levels of variability can be observed across the conditions. Conditions E and F exhibit narrower box plots, indicating lower dispersion, with values concentrated closer to the median. In contrast, condition G shows a higher degree of data dispersion. Additionally, outliers are observable in datasets B, C, and H, which can be attributed to potential anomalous measurements or natural variations in the data. The standard deviation is relatively high for the lamination conditions G (20.7) and H (26.7), indicating greater variability in the results. Except for condition B, which shows lower average values, conditions A, C, and D exhibit similar distributions as well as comparable mean and median values. In contrast, conditions E, F, G, and H display higher Gurley number values than the others, indicating an increasing trend due to the combined effects of higher lamination pressure and temperature.

Notably, the most marked increases in Gurley number are observed for the lamination conditions performed at 90 °C, suggesting that the temperature significantly influences both the process and the final properties of the separator. More specifically, an increase of more than 30 % of the Gurley number was observed for the lamination conditions F, G, and H.

A more in-depth statistical analysis using two-way ANOVA was conducted on a subset of the data to evaluate both the individual effects

Table 1
different lamination conditions for Al/separator/Al stack.

Sample name	Lamination speed mm s^{-1}	Lamination pressure N mm^{-1}	Lamination temperature °C
A	100	10	70
B	100	15	70
C	100	10	80
D	100	15	80
E	100	10	90
F	100	15	90
G	100	20	90
H	100	25	90

Table 2
Average Gurley number for Al/separator/Al stack subjected to different lamination conditions.

Sample name	Average Gurley number (s)	Standard deviation	% increase *vs* pristine
Pristine	318.6	14.1	–
A	371.3	13.6	16.5
B	340.3	14.0	6.8
C	360.7	17.1	13.2
D	371.4	14.8	16.6
E	396.4	8.2	24.4
F	423.9	8.1	33.1
G	432.6	20.7	35.8
H	493.3	26.7	54.8

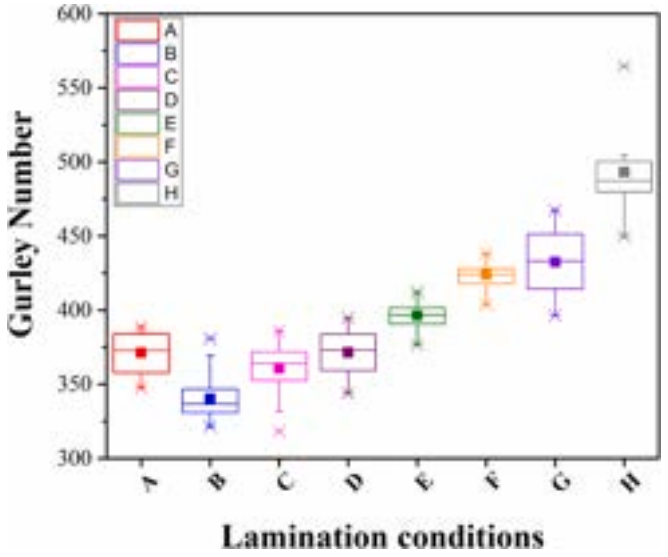

Fig. 1. Box chart of Gurley number for Al/separator/Al stack subjected to different lamination conditions: lower and upper fences are the 25th and 75th percentiles, bars include the ranges of 1.5IQR, full dots are the mean value, full lines are the median, and x are the outliers.

and the interaction of the two lamination parameters (pressure and temperature) on the Gurley number measured in the first area of each separator. For this analysis, two pressure values (10 and 15 N mm^{-1}) and three temperature values (70, 80, and 90 °C) were selected to ensure a coherent dataset. The results of the analysis are reported in Table S1.

The analysis revealed a significant effect of pressure on the Gurley number values ($F = 17.11$, $p = 0.000126$). This result suggests that the pressure variation has an evident statistical impact on the Gurley number (*e.g.* separator air permeability). Similarly, the effect of temperature was found to be highly significant ($F = 102.79$, $p < 0.0001$), demonstrating that temperature is a more impactful factor than pressure on the permeability variation of the separator. However, more interestingly, the analysis revealed a significant interaction between pressure and temperature ($F = 24.72$, $p = 2.6 \times 10^{-8}$), suggesting that the relationship between the two factors is not independent and their effects should be considered together.

In general, the air permeability decrease, as a consequence of the combined effect of pressure and temperature, is significant. However, it is important to underline that, in this case, aluminum sheets were used, and the results may not be directly comparable to analyses conducted with porous electrodes. Anyway, this pre-screening analysis is useful for excluding excessively extreme lamination conditions that could cause mechanical deformations in the separator, potentially leading to short circuits.

To confirm this, the morphology of the delaminated separators subjected to conditions A, F, and H was evaluated by FESEM analysis. In Fig. 2, the three delaminated separators are directly compared with the pristine separator at three different magnifications. The FESEM micrographs show that the pristine separator exhibits a homogeneous distribution of coalesced spherical binder particles (PVDF) on the surface. Some discontinuous areas are visible, revealing the characteristic morphology of the polyolefin separator and its characteristic porosity under the PVDF particles. In particular, the micrographs of the laminated separators reveal increased coalescence of the superficial PVDF particles, attributed to the combined effects of pressure and temperature. Interestingly, the underlying surface appears more stretched, indicating pores opening. While the morphology of separators subjected to lamination processes A and F remains similar, the stretching phenomenon is more pronounced in samples subjected to lamination H, which underwent the most extreme conditions presented in this study. It is important to note that multiple areas of each separator were examined, and for the separator subjected to lamination conditions H, small superficial fractures were observed. However, these fractures appear to be localized and superficial, supporting the hypothesis that they result from the natural pores opening during the lamination process, without compromising the overall structure or mechanical integrity of the separator. By better analysing and comparing the results from the permeability and morphological analyses of the delaminated separators, a dual effect of the lamination process on the separator can be hypothesized. On one hand, lamination softens the PVDF surface layer, causing its coalescence, and consequently reducing the separator air permeability. However, this effect is partially counterbalanced by the stretching of the underlying layer and the opening of new pores. This double effect of the lamination process can affect the properties of the separator, such as: ionic conductivity and electrical insulation. Therefore, these aspects were subsequently evaluated by means of electrochemical impedance spectroscopy and through the calculation of the MacMullin number.

More in detail, the impact of different lamination conditions on the ionic conductivity of the separator was evaluated by calculating the MacMullin number. For this analysis, separators laminated under conditions A and H were selected, as these samples exhibited the most significant differences both in terms of Gurley number and morphology. Typically, the MacMullin (N_m) number is the ratio between the resistivity of the pure electrolyte and the separator resistivity. So, N_m describes the relative contribution of a separator to cell resistance. In other words, the MacMullin number quantifies the ionic conductivity decrease caused by the separator, which is directly related to the separator porosity and tortuosity [34–36]. The resistance of varying numbers of separator layers (ranging from 1 to 3) placed between two blocking electrodes was measured using electrochemical impedance spectroscopy. By fitting the data, the resistances were determined in relation to the number of separator layers. The ionic resistance was calculated through the fitting of the EIS spectrum using the equivalent circuit shown in Fig. S2a, identifying the intercept point with the Z′ axis [36]. The linear regression of the resistance measured for each stack of separators provides the ratio $\Delta R_{ion}/\Delta N_{Layers}$, which was useful for calculating the ionic conductivity of the electrolyte-impregnated separator, taking into account the area and thickness of the separator. Then, the N_m for the different separators was directly obtained by calculating the ratio between the ionic conductivity of the pure electrolyte [37] (previously determined, Fig. S2b) and the conductivity of the electrolyte-impregnated separator. As expected and visible in Fig. 3, an increase in the number of separator layers (*i.e.* the thickness of the stack) leads to a higher R_{ion} and a linear relationship for all the samples.

In Table 3 are reported the N_m for the pristine separator and those subjected to the lamination conditions A and H. An increase in the MacMullin number is observed as a consequence of the lamination process. In fact, for lamination conditions H a higher N_m was observed, which still remained within the acceptable range. Indeed, as reported elsewhere, the MacMullin number can vary widely (typically between 4 and 20) and is strongly influenced by the specific separator/electrolyte combination [38–40].

Based on the results obtained from the pre-screening lamination tests, two lamination conditions were selected and applied on the anode/separator/cathode stack: A - 100 mm s^{-1}, 10 N mm^{-1} and 70 °C and H - 100 mm s^{-1}, 25 N mm^{-1} and 90 °C (Table S2). These two lamination conditions, which involve significantly different temperature and pressure values, enable better quantification of the process without compromising the materials. In fact, as shown by Leithoff et al. [20], temperatures $\leq$ 60 °C make the lamination process ineffective. Conversely, at temperatures $\geq$ 120 °C, the commercial trilayer separator undergoes structural damage. Analogously, starting from the conclusions of the same authors, the lamination speed was kept constant at 100 mm s^{-1}, since too low speeds lead to a significant decrease in electrical resistance and therefore a higher risk of short circuits.

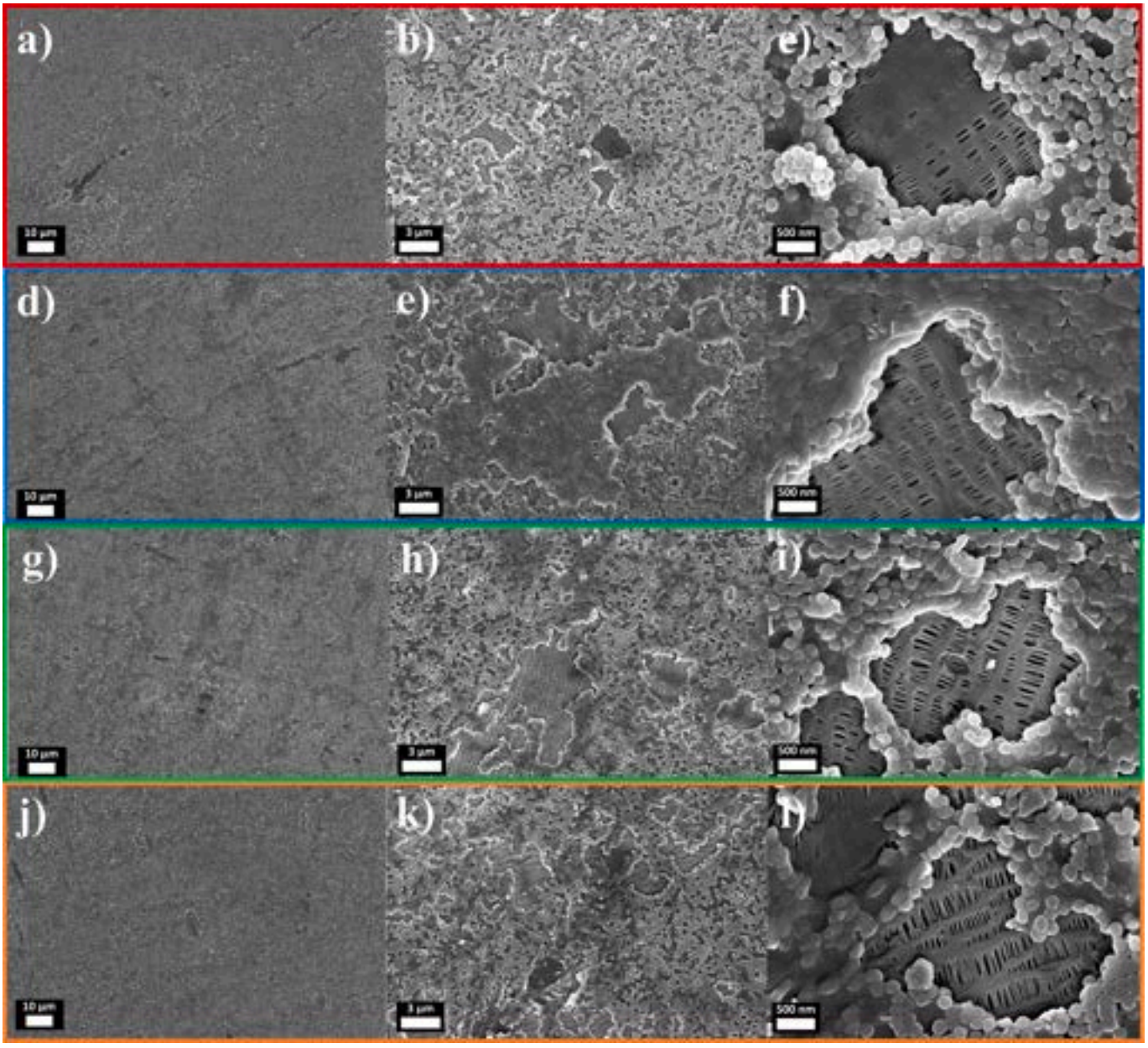

Fig. 2. FE-SEM micrographs of the pristine separator at 2kX (a), 10 kX (b), 50 kX (c); separator laminated under condition A at 2kX (d), 10 kX (e), 50 kX (f); separator laminated under condition F at 2kX (g), 10 kX (h), 50 kX (i); separator laminated under condition H at 2kX (j), 10 kX (k), 50 kX (l). Al/separator/Al stack configuration.

The Gurley analysis was repeated for the laminated stack anode-separators-cathode. For a direct comparison, the pristine separator was subjected to the same treatment. As shown in Table 4, the Gurley number increases with varying lamination conditions, ranging from approximately 12 % for condition A to 47 % for condition H. Taking into account that in this case two porous electrodes are laminated on the separator, these values are consistent with those obtained for the Al/separator/Al stack using the same lamination conditions.

Fig. 4 presents the micrographs of the separators laminated under conditions A and H after the de-lamination process in isopropanol, as described in the experimental section.

Both samples showed a greater presence of anodic material (graphite) on the delaminated separator. This is particularly evident in micrographs a–b and g–h, where graphite particles are clearly identifiable. On the side of the separator exposed to the cathode, a lower quantity of active material particles is observed compared to the anodic side. However, in this case, more pronounced craters left by the active material particles (NMC 811) are visible. At higher magnification, the PVDF particles appear more cohesive and fused together, while the underlying polyolefin layer exhibits a more stretched morphology. Similar to the laminated separators in the Al/separator/Al stack, no signs of separator breakage were detected, confirming that both lamination processes do not compromise the structural integrity of the separator. These observations confirm that there is a non-negligible effect of the morphology of the active materials and more generally of the electrode that needs to be taken into account during the lamination process.

In addition to the Gurley number, the MacMullin number was also calculated to further evaluate the impact of different lamination processes on the ionic conductivity of the separator. Following the same approach used for the laminated separators stacked with aluminum foils, the delaminated separators were impregnated with the electrolyte

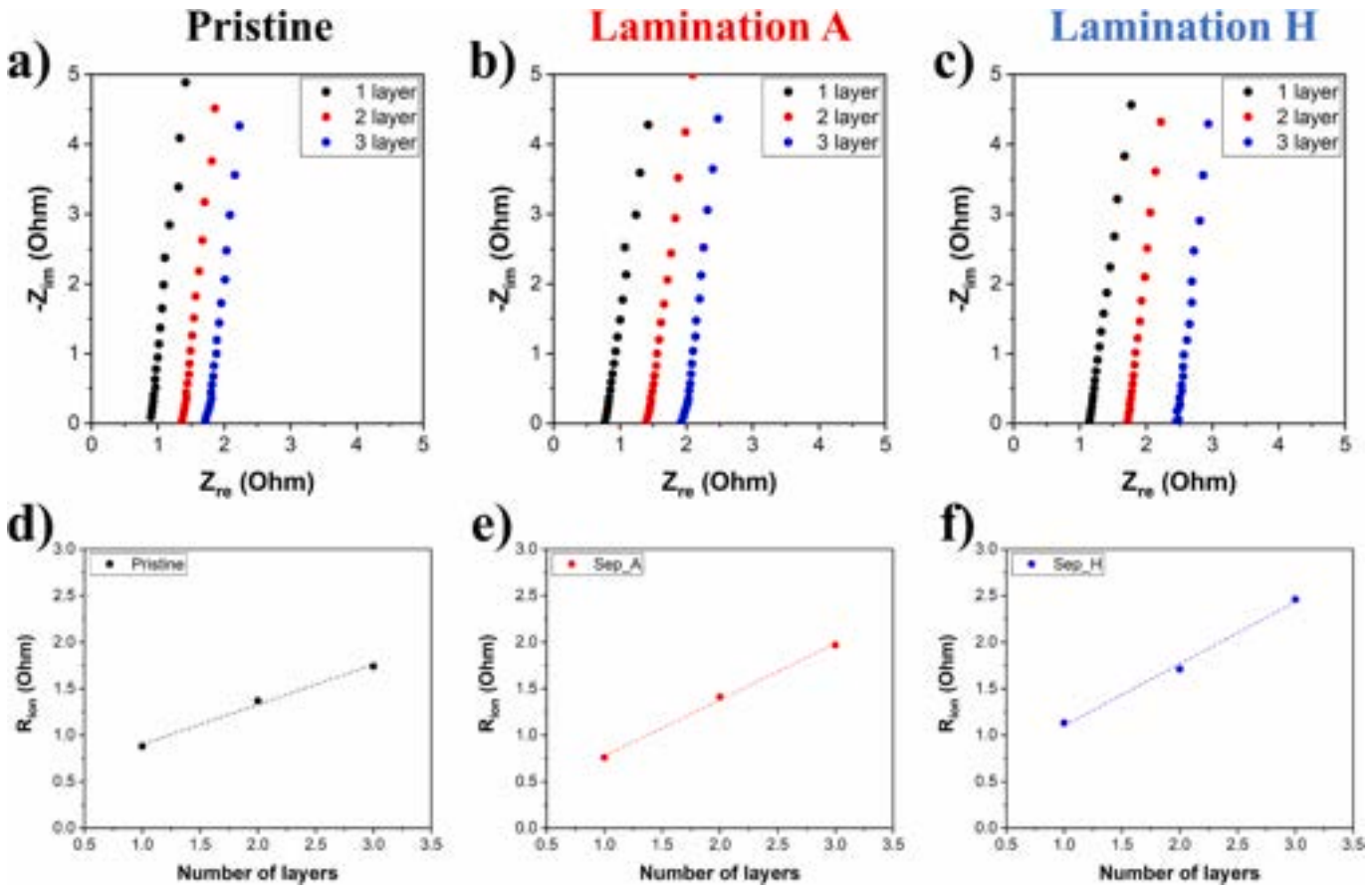

Fig. 3. Nyquist plots of the EIS measurements for the different laminated separators in Al/separator/Al stack configuration: pristine (A), lamination A (b), lamination H (c). Plot of the Rion values against the number of separator layers for pristine (d), lamination A (e), lamination H (f).

Table 3
MacMullin number comparison for pristine and laminated separator.

Sample name	Pristine	Lam. A	Lam. H
Area (cm^2)	2.54	2.54	2.54
Thickness (cm)	0.0020	0.0020	0.0020
$\Delta R_{ion}/\Delta N_{Layers}$ (ohm)	0.43	0.60	0.66
σ (mS cm^{-1})	1.65	1.18	1.07
N_M	4.61	6.44	7.10

Table 4
Average Gurley number for graphite/separator/NMC811 stack subjected to different lamination conditions.

Sample name	Average Gurley number (s)	Standard deviation	% increase *vs* pristine
Pristine	270.8	10.4	–
Lam. A	302.7	10.2	11.8
Lam. H	398.6	6.4	47.2

solution for 48 h. Their resistance was then measured using electrochemical impedance spectroscopy. To assess the correlation between resistance and the number of separator layers, measurements were conducted on stacks containing one to four separator layers (Fig. 5).

In general, an increase in the MacMullin number is observed as a function of the lamination conditions (Table 5). More specifically, an increase of 14 % in N_m is recorded for lamination condition A, whereas for condition H, the increase reaches 30 %. Therefore, even in absolute terms, the MacMullin number for both separators subjected to different lamination conditions remains within the critical applicability threshold. This confirms that both lamination conditions can be applied without detrimentally affecting the ionic conductivity of the system while still ensuring effective electronic isolation.

Nevertheless, to ensure that the lamination process did not compromise the separator electrical insulation, all laminated stacks were subjected to a HI-POT test [41]. All stacks were subjected to the same pressure as in the electrochemical tests (0.10 N mm^{-2}), and a potential of 500 V was applied for approximately 30 s. All stacks laminated under conditions A and H successfully passed the HI-POT test, demonstrating good electrical insulation of the system and excluding short circuits caused by excessive stretching of the separator.

Based on these results, all anode/separator/cathode stacks were used for subsequent electrochemical tests to assess the impact of different lamination conditions on the performance of lithium-ion cells. In fact, as also pointed out by Frankenberger et al. the effects of lamination can be evaluated, especially at higher C-rates only when the cell is fully laminated, from both interfaces [28]. All assembled cells, before the galvanostatic formation and cycling process, were subjected to a resting period, at open circuit voltage, monitoring the internal resistance of the system by an EIS analysis. The EIS analysis was performed after 1 h, 12 h, and 24 h from the assembly. A total rest time of 24 h was set for two main reasons: (I) to monitor the stability of the cell, and (II) to ensure sufficient time for the electrolyte to permeate into the pores of the separator and electrodes.

In general, all samples exhibited good stability during the rest phase, showing no significant variation in resistance after 24 h. As an example, the Nyquist spectrum of the most representative cell for each lamination condition is reported in Fig. 6a–c. The EIS behaviours of multiple cells were monitored, and for each cell, the Nyquist spectrum was fitted using the same equivalent circuit, reported in Fig. 6d.

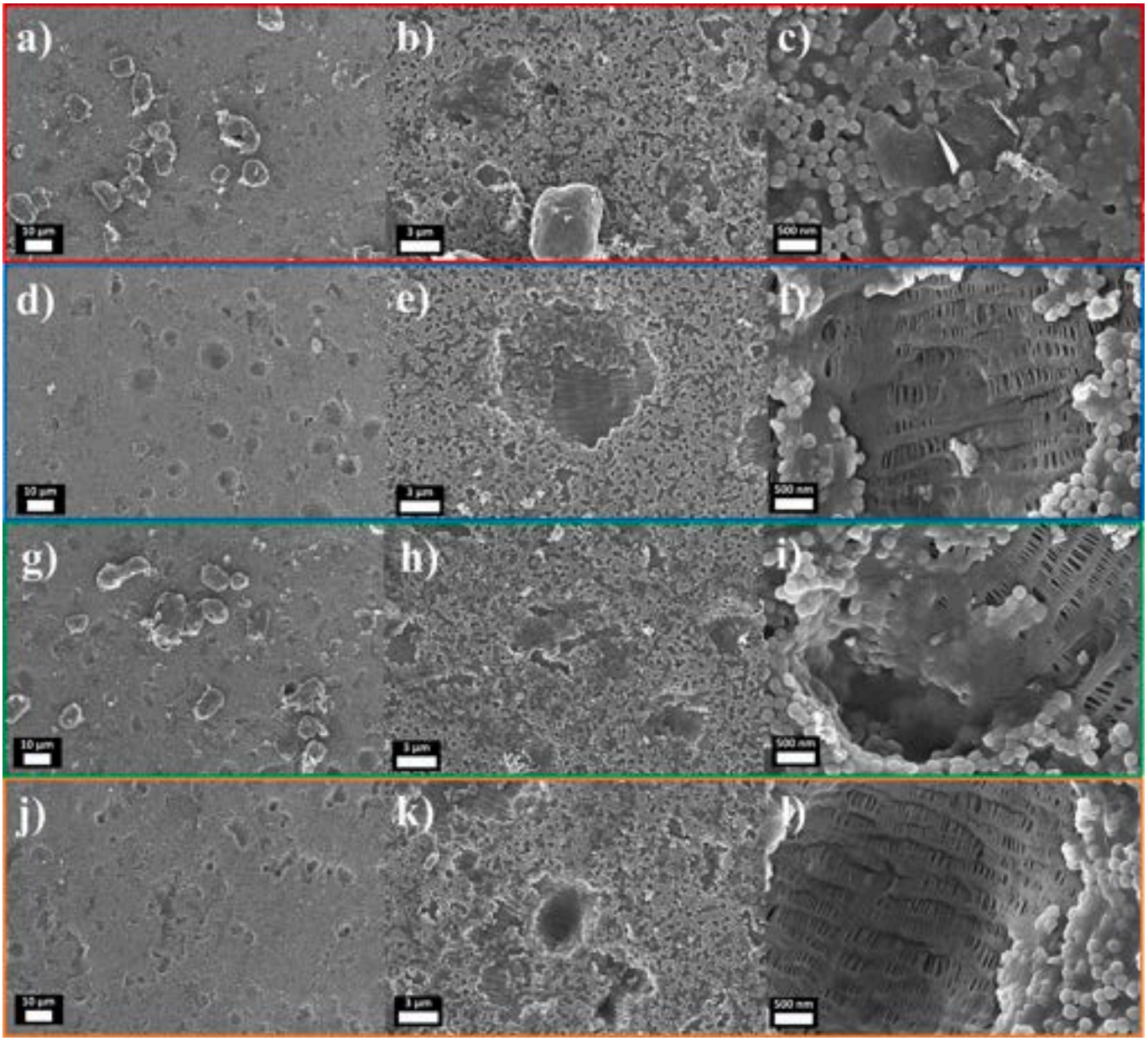

Fig. 4. FE-SEM micrographs of the laminated separator under condition A for anode side at 2kX (a), 10 kX (b), 50 kX (c) and cathode side at 2kX (d), 10 kX (e), 50 kX (f); separator under condition H for anode side at 2kX (g), 10 kX (h), 50 kX (i) and cathode side at 2kX (j), 10 kX (k), 50 kX (l). Anode/separator/cathode stack configuration.

At high frequencies, a resistance (R_{el}) can be identified, principally arising from the electrolyte resistance, with the contribution of inductive effects associated with the impedance measurement environment. At lower frequencies, a single dominant semicircle can be observed, as expected for non-cycled cells. This semicircle can be attributed to the overall charge transfer reactions (R_{ct}) occurring at both the anode and cathode sides. The mean values of R_{el} and R_{ct}, and the relative standard deviation, are reported in Table S3. R_{el} remains comparable and exhibits minimal variation across all samples, including both the non-laminated stack and the laminated samples under different conditions. The R_{el} value is below 1.5 Ω for all samples, appearing almost identical between the pristine sample and the sample laminated under condition A, while it was slightly higher for the sample laminated under condition H. This slight difference aligns with the MacMullin analyses, confirming that the lamination process does not negatively impact the R_{el} resistance. Conversely, R_{ct} is nearly identical for the pristine sample and the sample laminated with condition A, whereas it is higher for the sample laminated under condition H. Additionally, it is noteworthy that the sample subjected to lamination A exhibits lower data dispersion, indicating reduced variability in R_{ct} values. On the contrary, the R_{ct} values found for the pristine and laminated samples with H conditions show a higher standard deviation and therefore a higher variability of the data (Fig. 6e).

Subsequently, to the pre-forming phase, all the cells were subjected to a galvanostatic cycling process, including a forming step at low currents (0.1C), a rate capability test at different C-rates, and extended cycling at constant current equal to 1C for 100 cycles (useful for evaluating capacity retention). A lower current forming process (0.1C) was chosen to better understand the SEI layer formation process and stabilize the cell, in agreement with what was observed by Frankenberger et al. [27]. Five cells were analysed for each lamination condition, and the values were averaged to enhance statistical significance. Focusing on

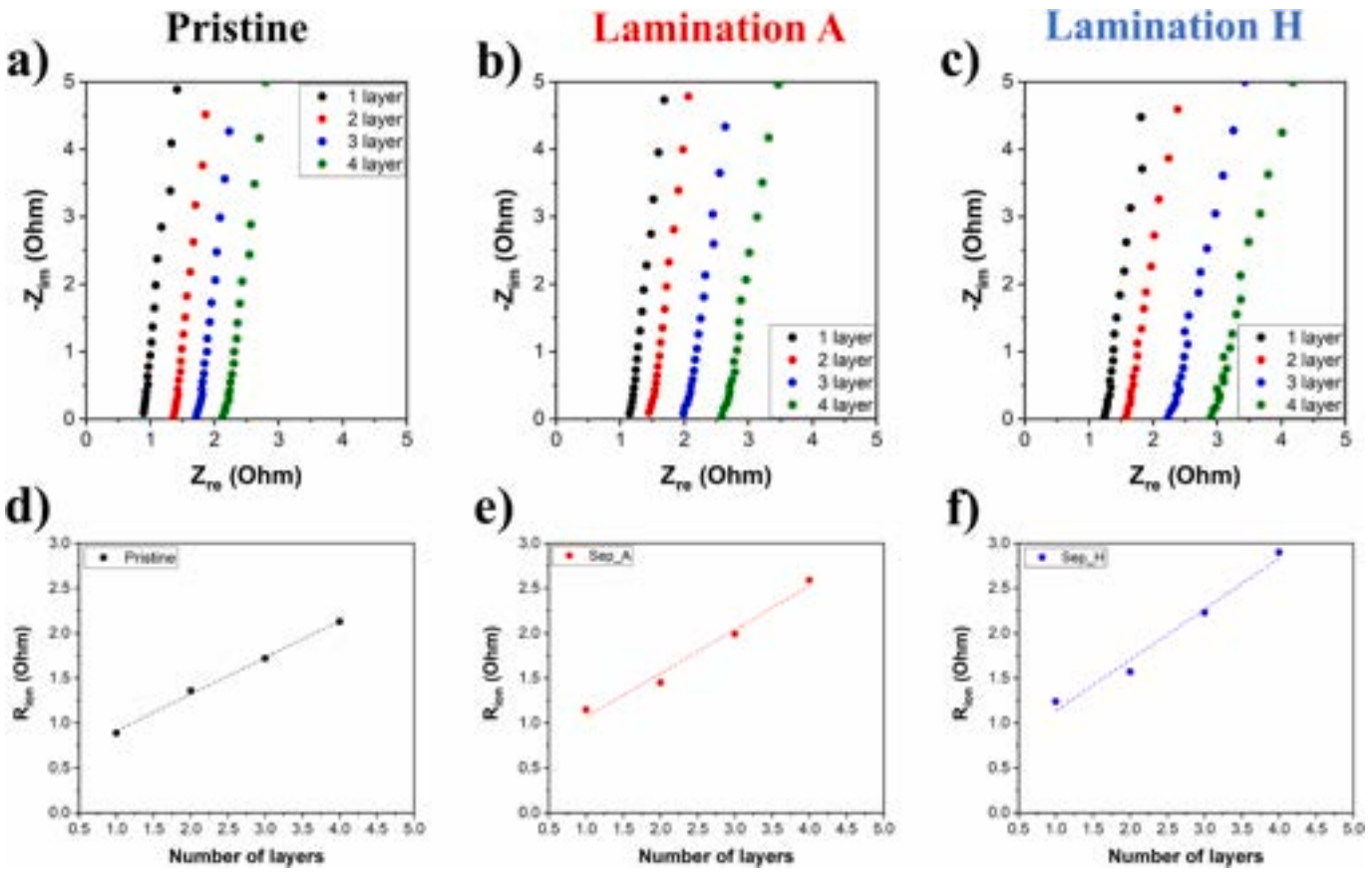

Fig. 5. Nyquist plots of the EIS measurements for the different laminated separators in anode/separator/cathode stack configuration: pristine (A), lamination A (b), lamination H (c). Plot of the Rion values against the number of separator layers for pristine (d), lamination A (e), lamination H (f).

Table 5
MacMullin number comparison for pristine and laminated separator in anode/separator/cathode stack configuration.

Sample name	Pristine	Lam. A	Lam. H
Area (cm^2)	2.54	2.54	2.54
Thickness (cm)	0.0020	0.0020	0.0020
$\Delta R_{ion}/\Delta N_{Layers}$ (ohm)	0.43	0.49	0.56
σ (mS cm^{-1})	1.69	1.48	1.30
N_M	4.50	5.13	5.85

forming cycles and, in particular, on the reversibility of the first cycle, from the box chart (Fig. 7a), it is evident that the pristine cells exhibit a wide interquartile range, indicating greater variability compared to the laminated samples, along with the presence of outlier values. For pristine samples, the average initial Coulombic efficiency (I.C.E.) value is close to 70 %, suggesting a more pronounced irreversibility of the electrochemical process during the first charge-discharge cycle. In contrast, for the lamination condition A, the box is narrower, reflecting lower data variability and an average I.C.E. value close to the median (~75 %). Meanwhile, for the lamination condition H, the interquartile range is both narrower and symmetrical, indicating low variability and, consequently, more reproducible I.C.E. values. Additionally, the I.C.E. values for condition H are higher than those observed for both the pristine and A samples. The general higher I.C.E. values observed for the laminated samples align with the findings of Frankenberger et al. [26,27], confirming that the lamination process enhances the stability of the SEI layer. This stabilization helps to limit lithium consumption, as well as the overall depletion of active material and electrolyte, which typically occurs during the initial forming cycles of the cell. This aspect is particularly important, as improved reversibility from the first cycles contributes to higher capacity and better capacity retention in subsequent cycles. By closely analysing the five formation cycles, a progressive increase in discharge capacity can be observed during the first 3–4 cycles. This activation process is particularly evident in the pristine and A-laminated samples but is nearly absent in the H-laminated cells. This behaviour suggests that, under more extreme lamination conditions, the cell appears to require less activation time, allowing the active material to be fully available for electrochemical processes from the beginning. These observations confirmed what was reported by Kaden et al. [25], who observed improved wettability of the laminated stack with the electrolyte, especially under stronger lamination conditions and at an applied temperature of 80 °C. A more pronounced lamination condition enhances the interconnections between the separator and the electrodes, facilitated by PVDF, which helps to form an ionically conductive network and promotes better electrolyte wettability.

Moving forward and analysing the average results obtained for the three samples during cycling at different C-rates (Fig. 7b–e and Table 6), a generally improved rate capability behaviour is observed for the laminated samples. In particular, the non-laminated pristine samples exhibit greater data dispersion, indicating higher variability in performance. Additionally, the average initial capacity is lower if compared to the laminated samples, and a more pronounced drop in areal capacity is observed as the C-rate increases. Conversely, for the laminated samples under condition A, a higher initial capacity is observed compared to the non-laminated samples, with a more stable capacity retention. Additionally, lower data variability is noted, particularly at higher C-rates, confirming an improved reproducibility of the electrochemical performance. A similar trend is observed for the samples laminated under condition H, which exhibit an initial capacity close to the maximum value of 2.0 mAh cm^{-2}. As reported in Table 6, at higher C-rates, the specific capacity is higher for cells laminated under condition A than for

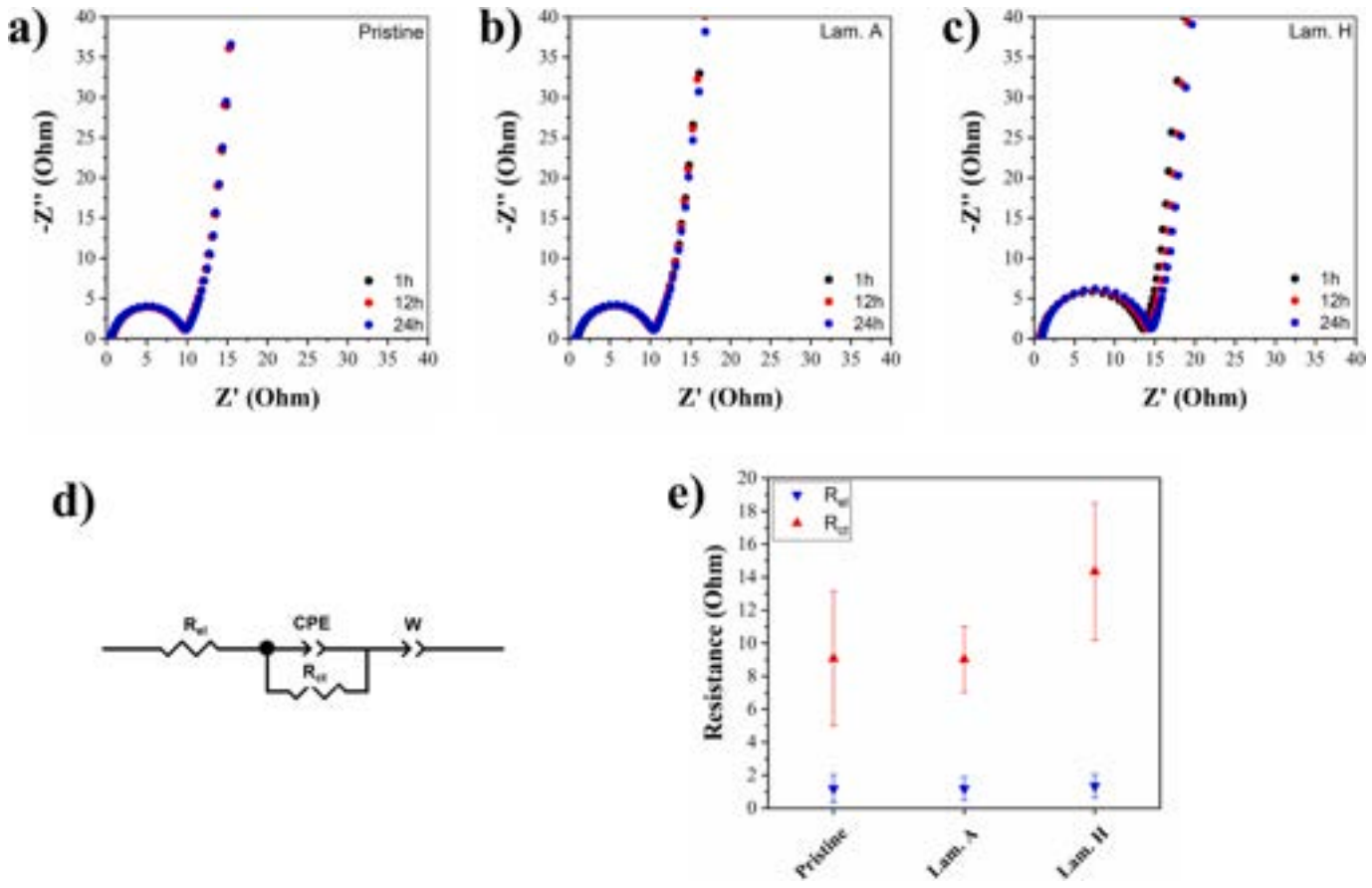

Fig. 6. Representative Nyquist plots obtained anode/separator/cathode stack configuration for pristine condition (a), lamination condition A (b), lamination condition H (c), equivalent circuit model used for fitting (d), and direct comparison of average R_{el} and R_{ct} (e).

cells laminated under condition H. This observation is consistent with the PEIS and MacMullin analyses performed after electrolyte infiltration (Figs. 5 and 6), which show that cells prepared under condition H exhibit higher total resistance compared to those under condition A. Nevertheless, this higher resistance does not negatively impact capacity retention, and remains consistently higher than the pristine sample for all the C-rates.

The higher initial specific capacity is also supported by enhanced rate capability and greater reproducibility, particularly at low C-rates. According to the results, a higher Coulombic efficiency during the initial forming cycles (C/10) translates into greater specific capacity and improved capacity retention. At the same time, the higher resistance observed in the EIS analysis for the laminated samples does not appear to negatively impact or compromise their electrochemical performance at higher C-rates.

After the rate capability test, the samples were subjected to a long-term cycling test (100 cycles) at a constant current of 1C. As shown in Fig. 7f–h, the specific capacity values are lower for the non-laminated cells. Additionally, these samples exhibit greater variability during the 100 cycles, compared to the laminated ones. In fact, for lamination condition A, a higher and more stable capacity is observed over the 100 cycles at 1C, with reduced variability. Similar trends are noted for lamination condition H, which demonstrates the best performance in terms of stability, exhibiting a lower capacity decay, lower variability, and better reproducibility.

To obtain a more comprehensive understanding of the average capacity retention for each lamination condition, the capacity values obtained at low C-rates (C/10) during the fifth formation cycle, after the rate capability test (25th cycle), and at the end of the long cycle (final C/10 cycle following 100 cycles at 1C), were calculated and reported in Table S4. Directly comparing the average capacity at 25th cycle to the 5th cycle, all three samples exhibit a similar capacity retention of approximately 96 %. However, the differences among the three samples become more evident if the capacity is compared between the 130th cycle and the 5th cycle: in this case, the average capacity retention for the non-laminated samples is 54 %, whereas, for the laminated samples, it is 72 % for condition A and 79 % for condition H. This confirms that, despite the differences in terms of capacity, the irreversible capacity loss after the rate capability test is comparable for all the samples. However, prolonged cycling at higher C-rates (1C) reveals a greater capacity decay for the pristine condition, reinforcing the beneficial effect of the lamination process on cell cyclability and lifespan. While comparing the two lamination conditions, the H samples exhibit better stability during the first cycles but also after the prolonged cycling at 1C, supporting the consideration that higher I.C.E. brings to higher capacity retention.

Fig. 8 reports the charge and discharge profiles of three cells, each corresponding to a different lamination condition. The selected cells were chosen as the closest to the average values for their respective lamination conditions.

As observed in the charge/discharge profiles, the pristine sample exhibits greater polarization phenomena, in comparison to the samples laminated under conditions A and H. This increased polarization is evident for all the C-rates but becomes more pronounced as the charge/discharge rate increases. This is also evident from the contribution of the constant voltage step to the overall capacity. In general, increased polarization in charge/discharge profiles is indicative of higher internal resistance, confirming that the lamination process helps to mitigate the polarization effect.

Overall, these findings demonstrate that the lamination process plays a critical role in tailoring the final electrochemical performance. On one

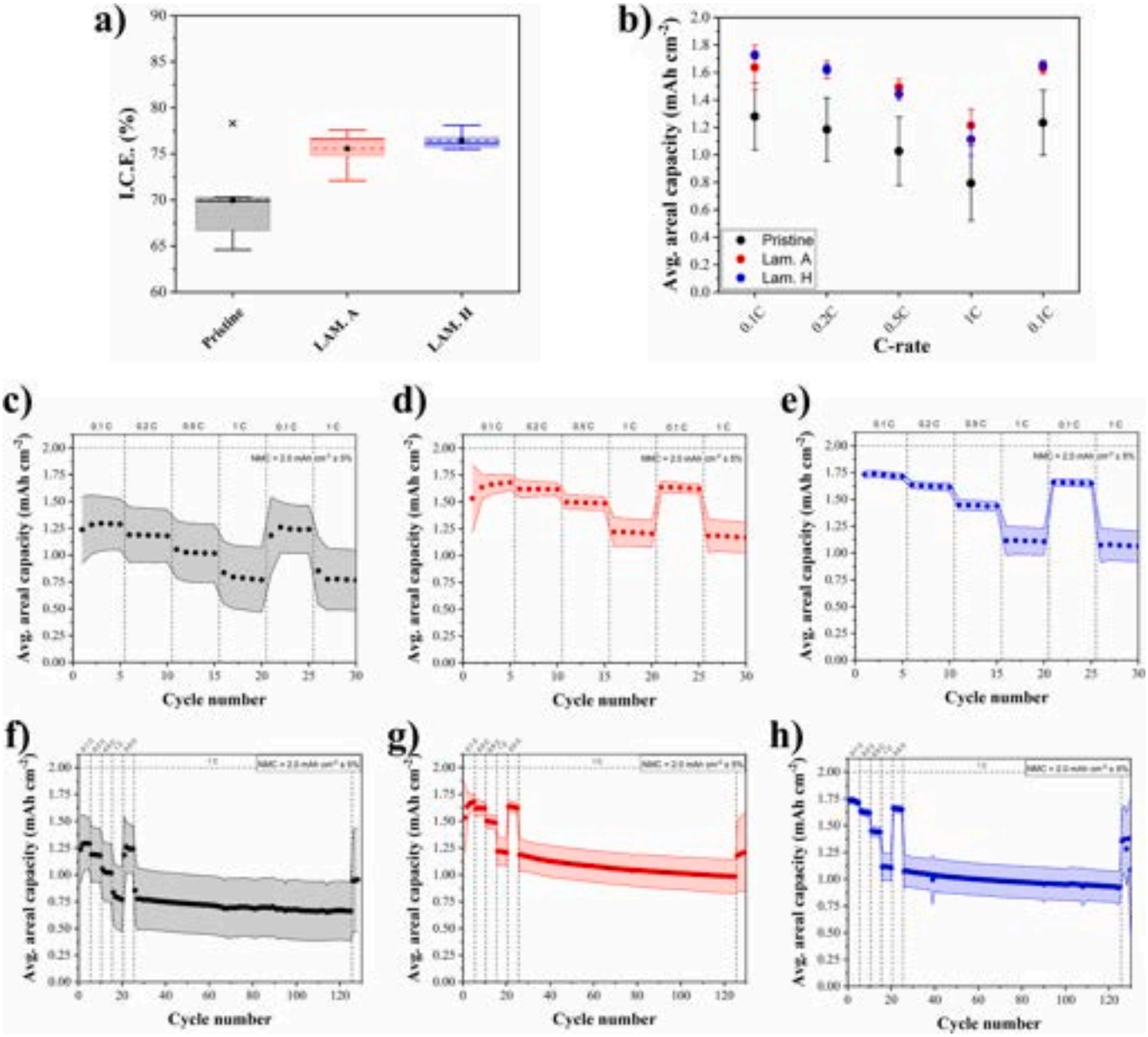

Fig. 7. Box chart of I.C.E. for cell containing anode/separator/cathode stack subjected to different lamination conditions (a). Average discharge capacity direct comparison for rate capability test, performed at RT (25 ± 2 °C) (b). Rate capability results averaged over 5 cells for pristine condition (c), lamination condition A (d), and lamination condition H (e). Long cycling performance at 1C performed at RT (25 ± 2 °C) for pristine condition (f), lamination condition A (g), and lamination condition H (h), averaged over 5 cells.

Table 6
Average discharge capacity (over 5 cells), for the rate capability test of the three different lamination conditions for anode/separator/cathode stack configuration.

C-rate	Average discharge capacity mAh cm^{-2}		
	Pristine	Lam. A	Lam. H
0.1 $C_{initial}$	1.28 ± 0.24	1.64 ± 0.16	1.73 ± 0.03
0.2C	1.18 ± 0.23	1.62 ± 0.06	1.62 ± 0.03
0.5C	1.03 ± 0.25	1.49 ± 0.06	1.44 ± 0.04
1C	0.79 ± 0.27	1.21 ± 0.12	1.11 ± 0.12
0.1 C_{final}	1.23 ± 0.24	1.63 ± 0.04	1.65 ± 0.03

hand, more extreme lamination (as in condition H) may reduce separator ionic conductivity, increasing internal resistance and affecting rate capability. On the other hand, it may improve the electrode/separator interface, promoting the formation and stability of SEI and CEI layers, which contributes to enhanced ICE and long-term capacity retention. These results highlight the need to tailor the lamination process to the specific electrode materials to obtain an optimal balance between rate performance and cycle life.

4. Conclusion

With the growing demand for lithium-ion batteries, optimizing the cell manufacturing process has become increasingly critical. However, the LIBs manufacturing process is complex, involving several sequential steps, each with its challenges. One of the most crucial step, at the industrial level, is the electrode/separator stacking process, which often

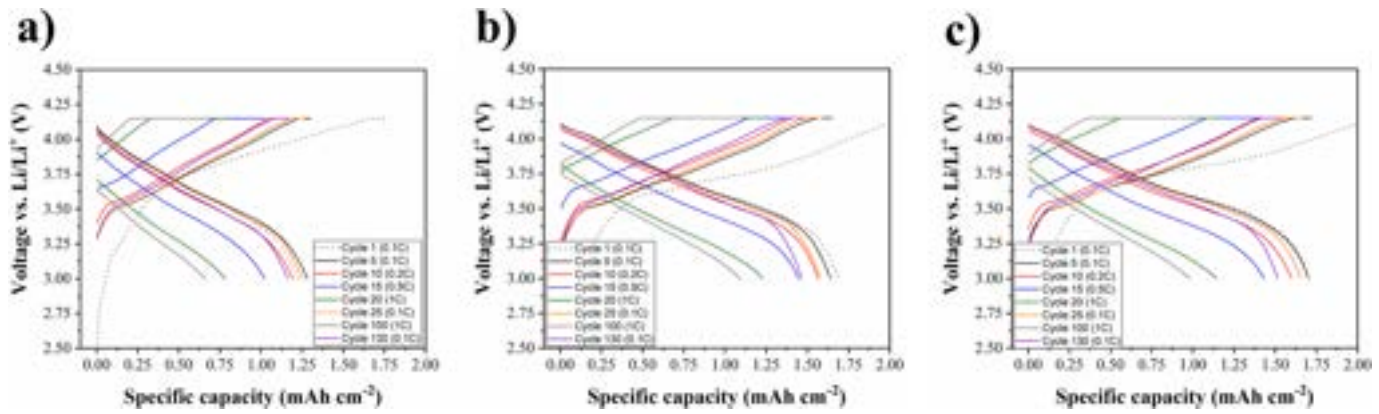

Fig. 8. Charge/discharge profiles for representative cell: pristine (a), lamination condition A (b), and lamination condition H (c) for anode/separator/cathode stack configuration.

includes a lamination step. This step plays a key role, as it significantly affects both the cost and efficiency of manufacturing, influencing at the same time the final performance of the cells. Therefore, studying and optimizing the lamination process is essential, not only to reduce manufacturing scrap, but also to enhance critical battery properties such as capacity retention and rate capability. In the present study, we aimed to evaluate the impact of different lamination conditions on the electrochemical performance of NMC811/graphite pouch cells. The statistical study of the results allowed to identify the combined effect of pressure and temperature and, at the same time, to identify the two most interesting lamination conditions applicable to the full anode/separator/cathode stack.

Cells assembled with laminated stacks exhibited enhanced electrochemical performance compared to the non-laminated (pristine) configuration. Laminated cells demonstrated improved rate capability, delivering higher capacity values at higher C-rates. Additionally, the lamination led to better capacity retention after prolonged cycling at a fixed C-rate of 1C. Interestingly, higher lamination pressure and temperature conditions resulted in a higher I.C.E. and a more stable Coulombic efficiency from the first forming cycles. This suggests improved electrolyte wettability of the separator and the formation of a more uniform and stable SEI layer, despite a slight decreasing of the separator permeability and ionic conductivity. These aspects were also reflected in the overall system stability, characterized by lower data dispersion and better capacity retention, particularly after extended cycling.

This highlights the importance of further research on the lamination process, even at a laboratory scale. In fact, a deeper understanding of the lamination process, combined with a more in-depth study of the effect on the materials, could lead to enhanced electrochemical performance, manufacturing process optimization, cost reduction, and a significant reduction in production scrap.

CRediT authorship contribution statement

Daniele Versaci: Writing – original draft, Visualization, Validation, Methodology, Investigation, Funding acquisition, Data curation, Conceptualization. **Silvio Fugattini:** Writing – review & editing, Validation, Methodology, Investigation, Funding acquisition, Conceptualization. **Michele Serri:** Writing – review & editing, Validation, Methodology, Investigation, Funding acquisition, Conceptualization. **Andrea Moselli:** Writing – review & editing, Validation, Methodology, Investigation, Funding acquisition, Conceptualization. **Julia Amici:** Writing – review & editing, Supervision, Resources, Investigation, Funding acquisition. **Silvia Bodoardo:** Writing – review & editing, Supervision, Resources, Funding acquisition.

Declaration of competing interest

The authors declare that they have no known competing financial interests or personal relationships that could have appeared to influence the work reported in this paper.

Acknowledgements

Daniele Versaci acknowledges support from FSE REACT-EU - PON Ricerca e Innovazione 2014–2020 program (Ministerial Decree no. 1062/2021).

Appendix A. Supplementary data

Supplementary data to this article can be found online at https://doi.org/10.1016/j.est.2025.118584.

Data availability

Data will be made available on request.

References

[1] S. Passerini, L. Barelli, M. Baumann, J.F. Peters, M. Weil, Emerging Battery Technologies to Boost the Clean Energy Transition, Springer International Publishing, Cham, 2024, https://doi.org/10.1007/978-3-031-48359-2.
[2] M.A. Hannan, A.Q. Al-Shetwi, R.A. Begum, P. Jern Ker, S.A. Rahman, M. Mansor, M.S. Mia, K.M. Muttaqi, Z.Y. Dong, Impact assessment of battery energy storage systems towards achieving sustainable development goals, J. Energy Storage 42 (2021) 103040, https://doi.org/10.1016/j.est.2021.103040.
[3] D. Bresser, D. Buchholz, A. Moretti, A. Varzi, S. Passerini, Alternative binders for sustainable electrochemical energy storage – the transition to aqueous electrode processing and bio-derived polymers, Energy Environ. Sci. 11 (2018) 3096–3127, https://doi.org/10.1039/C8EE00640G.
[4] J. Amici, P. Asinari, E. Ayerbe, P. Barboux, P. Bayle-Guillemaud, R.J. Behm, M. Berecibar, E. Berg, A. Bhowmik, S. Bodoardo, I.E. Castelli, I. Cekic-Laskovic, R. Christensen, S. Clark, R. Diehm, R. Dominko, M. Fichtner, A.A. Franco, A. Grimaud, N. Guillet, M. Hahlin, S. Hartmann, V. Heiries, K. Hermansson, A. Heuer, S. Jana, L. Jabbour, J. Kallo, A. Latz, H. Lorrmann, O.M. Løvvik, S. Lyonnard, M. Meeus, E. Paillard, S. Perraud, T. Placke, C. Punckt, O. Raccurt, J. Ruhland, E. Sheridan, H. Stein, J.M. Tarascon, V. Trapp, T. Vegge, M. Weil, W. Wenzel, M. Winter, A. Wolf, K. Edström, A roadmap for transforming research to invent the batteries of the future designed within the European large scale research initiative BATTERY 2030+, Adv. Energy Mater. 12 (2022) 2102785 https://doi.org/10.1002/AENM.202102785.
[5] R. Schmuch, R. Wagner, G. Hörpel, T. Placke, M. Winter, Performance and cost of materials for lithium-based rechargeable automotive batteries, Nat. Energy 3 (2018) 267–278, https://doi.org/10.1038/s41560-018-0107-2.
[6] M. Armand, P. Axmann, D. Bresser, M. Copley, K. Edström, C. Ekberg, D. Guyomard, B. Lestriez, P. Novák, M. Petranikova, W. Porcher, S. Trabesinger, M. Wohlfahrt-Mehrens, H. Zhang, Lithium-ion batteries – current state of the art and anticipated developments, J. Power Sources 479 (2020) 228708, https://doi.org/10.1016/J.JPOWSOUR.2020.228708.
[7] E. Ravesio, A.H.A. Lutey, D. Versaci, L. Romoli, S. Bodoardo, Nanosecond pulsed laser texturing of Li-ion battery electrode current collectors: electrochemical

characterisation of cathode half-cells, Sustain. Mater. Technol. 38 (2023) e00751, https://doi.org/10.1016/j.susmat.2023.e00751.
[8] D. Spada, B. Albini, P. Galinetto, D. Versaci, C. Francia, S. Bodoardo, G. Bais, M. Bini, FeNb11O29, anode material for high-power lithium-ion batteries: pseudocapacitance and symmetrisation unravelled with advanced electrochemical and in situ/operando techniques, Electrochim. Acta 393 (2021), https://doi.org/10.1016/j.electacta.2021.139077.
[9] Z. Tan, X. Chen, Y. Li, X. Xi, S. Hao, X. Li, X. Shen, Z. He, W. Zhao, Y. Yang, Enabling superior cycling stability of LiNi0.9Co0.05Mn0.05O2 with controllable internal strain, Adv. Funct. Mater. 33 (2023) 2215123, https://doi.org/10.1002/ADFM.202215123;SUBPAGE:STRING:ABSTRACT;REQUESTEDJOURNAL:JOURNAL:16163028;WGROUP:STRING:PUBLICATION.
[10] Z. Tan, X. Chen, J. Lin, Y. Huang, W. Cheng, Q. Liu, H. Zhang, F. Ren, Y. Huang, Z. Liu, T. Brezesinski, Y. Yang, W. Zhao, Restraining planar gliding in single-crystalline LiNi0.9Co0.05Mn0.05O2 cathodes by combining bulk and surface modification strategies, Angew. Chem. Int. Ed. 64 (2025) e202419903, https://doi.org/10.1002/ANIE.202419903.
[11] W. Zhao, K. Wang, R. Dubey, F. Ren, E. Brack, M. Becker, R. Grissa, L. Seidl, F. Pagani, K. Egorov, K.V. Kravchyk, M.V. Kovalenko, P. Yan, Y. Yang, C. Battaglia, Extending the high-voltage operation of graphite/NCM811 cells by constructing a robust electrode/electrolyte interphase layer, Mater. Today Energy 34 (2023) 101301, https://doi.org/10.1016/J.MTENER.2023.101301.
[12] P.S. Grant, D. Greenwood, K. Pardikar, R. Smith, T. Entwistle, L.A. Middlemiss, G. Murray, S.A. Cussen, M.J. Lain, M.J. Capener, M. Copley, C.D. Reynolds, S. D. Hare, M.J.H. Simmons, E. Kendrick, S.P. Zankowski, S. Wheeler, P. Zhu, P. R. Slater, Y.S. Zhang, A.R.T. Morrison, W. Dawson, J. Li, P.R. Shearing, D.J.L. Brett, G. Matthews, R. Ge, R. Drummond, E.C. Tredenick, C. Cheng, S.R. Duncan, A. M. Boyce, M. Faraji-Niri, J. Marco, L.A. Roman-Ramirez, C. Harper, P. Blackmore, T. Shelley, A. Mohsseni, D.J. Cumming, Roadmap on Li-ion battery manufacturing research, J. Phys. Energy 4 (2022) 042006, https://doi.org/10.1088/2515-7655/ac8e30.
[13] Y. Liu, R. Zhang, J. Wang, Y. Wang, Current and future lithium-ion battery manufacturing, IScience 24 (2021) 102332, https://doi.org/10.1016/j.isci.2021.102332.
[14] A. Kwade, W. Haselrieder, R. Leithoff, A. Modlinger, F. Dietrich, K. Droeder, Current status and challenges for automotive battery production technologies, Nat. Energy 3 (2018) 290–300, https://doi.org/10.1038/s41560-018-0130-3.
[15] R. Gonçalves, S. Lanceros-Méndez, C.M. Costa, Electrode fabrication process and its influence in lithium-ion battery performance: state of the art and future trends, Electrochem. Commun. 135 (2022) 107210, https://doi.org/10.1016/j.elecom.2022.107210.
[16] J.T. Frith, M.J. Lacey, U. Ulissi, A non-academic perspective on the future of lithium-based batteries, Nat. Commun. 14 (2023) 420, https://doi.org/10.1038/s41467-023-35933-2.
[17] S. Dühnen, J. Betz, M. Kolek, R. Schmuch, M. Winter, T. Placke, Toward green battery cells: perspective on materials and technologies, Small Methods 4 (2020), https://doi.org/10.1002/smtd.202000039.
[18] L. Gaines, Y. Wang, How to maximize the value recovered from Li-ion batteries: hydrometallurgical or direct recycling? Electrochem. Soc. Interface 30 (2021) 51–54, https://doi.org/10.1149/2.F07213F.
[19] L. Yu, Y. Bai, B. Polzin, I. Belharouak, Unlocking the value of recycling scrap from Li-ion battery manufacturing: challenges and outlook, J. Power Sources 593 (2024) 233955, https://doi.org/10.1016/j.jpowsour.2023.233955.
[20] R. Leithoff, A. Fröhlich, S. Masuch, G. Ventura Silva, K. Dröder, Process-product interdependencies in lamination of electrodes and separators for lithium-ion batteries, Energies (Basel) 15 (2022) 2670, https://doi.org/10.3390/en15072670.
[21] S. Choi, N. Kim, D. Jin, Y. Roh, D. Kang, H. Lee, S.-T. Hong, H. Lee, Y.M. Lee, Systematic study on Li dendrite growth and suppression in pouch-type lithium-ion batteries with misaligned electrode pairs, J. Power Sources 579 (2023) 233265, https://doi.org/10.1016/j.jpowsour.2023.233265.
[22] L. Kong, R. Aalund, M. Alipour, S.I. Stoliarov, M. Pecht, Evaluating the manufacturing quality of lithium ion pouch batteries, J. Electrochem. Soc. 169 (2022) 040541, https://doi.org/10.1149/1945-7111/ac6539.
[23] F. Dai, M. Cai, Best practices in lithium battery cell preparation and evaluation, Commun. Mater. 3 (2022) 64, https://doi.org/10.1038/s43246-022-00286-8.
[24] A. du Baret de Limé, T. Lein, S. Maletti, K. Schmal, S. Reuber, C. Heubner, A. Michaelis, Impact of electrode defects on battery cell performance: a review, Batter. Supercaps 5 (2022) e202200239, https://doi.org/10.1002/batt.202200239.
[25] N. Kaden, N. Schlüter, R. Leithoff, S. Savas, S. Grundmeier, K. Dröder, Influence of the lamination process on the wetting behavior and the wetting rate of lithium-ion batteries, Processes 9 (2021) 1851, https://doi.org/10.3390/pr9101851.
[26] M. Frankenberger, M. Singh, A. Dinter, K.-H. Pettinger, EIS study on the electrode-separator interface lamination, Batteries 5 (2019) 71, https://doi.org/10.3390/batteries5040071.
[27] M. Frankenberger, M. Trunk, S. Seidlmayer, A. Dinter, J. Dittloff, L. Werner, R. Gernhäuser, Z. Revay, B. Märkisch, R. Gilles, K.-H. Pettinger, SEI growth impacts of lamination, formation and cycling in lithium ion batteries, Batteries 6 (2020) 21, https://doi.org/10.3390/batteries6020021.
[28] M. Frankenberger, M. Singh, A. Dinter, S. Jankowksy, A. Schmidt, K.-H. Pettinger, Laminated lithium ion batteries with improved fast charging capability, J. Electroanal. Chem. 837 (2019) 151–158, https://doi.org/10.1016/j.jelechem.2019.02.030.
[29] Test Method for Resistance of Nonporous Paper to Passage of Air, 1999, https://doi.org/10.1520/D0726-94R99.
[30] M.F. Lagadec, R. Zahn, V. Wood, Characterization and performance evaluation of lithium-ion battery separators, Nat. Energy 4 (2018) 16–25, https://doi.org/10.1038/s41560-018-0295-9.
[31] V. Deimede, C. Elmasides, Separators for lithium-ion batteries: a review on the production processes and recent developments, Energy Technol. 3 (2015) 453–468, https://doi.org/10.1002/ente.201402215.
[32] P. Arora, Z.J. Zhang, Battery separators, Chem. Rev. 104 (2004) 4419–4462, https://doi.org/10.1021/cr020738u.
[33] Y. Lee, J. Park, H. Jeon, D. Yeon, B.-H. Kim, K.Y. Cho, M.-H. Ryou, Y.M. Lee, In-depth correlation of separator pore structure and electrochemical performance in lithium-ion batteries, J. Power Sources 325 (2016) 732–738, https://doi.org/10.1016/j.jpowsour.2016.06.094.
[34] D.V. Horváth, R. Tian, C. Gabbett, V. Nicolosi, J.N. Coleman, Quantifying the effect of separator thickness on rate performance in lithium-ion batteries, J. Electrochem. Soc. 169 (2022) 030503, https://doi.org/10.1149/1945-7111/ac5654.
[35] C. Sauter, R. Zahn, V. Wood, Understanding electrolyte infilling of lithium ion batteries rights/license: creative commons attribution 4.0 international funding acknowledgement: 680070-development of quantitative metrologies to guide lithium ion battery manufacturing (EC), J. Electrochem. Soc. 167 (2020), https://doi.org/10.3929/ethz-b-000426689.
[36] D. Parikh, T. Christensen, C.-T. Hsieh, J. Li, Elucidation of separator effect on energy density of Li-ion batteries, J. Electrochem. Soc. 166 (2019) A3377–A3383, https://doi.org/10.1149/2.0571914jes.
[37] A.J. Ringsby, K.D. Fong, J. Self, H.K. Bergstrom, B.D. McCloskey, K.A. Persson, Transport phenomena in low temperature lithium-ion battery electrolytes, J. Electrochem. Soc. 168 (2021) 080501, https://doi.org/10.1149/1945-7111/ac1735.
[38] J. Landesfeind, J. Hattendorff, A. Ehrl, W.A. Wall, H.A. Gasteiger, Tortuosity determination of battery electrodes and separators by impedance spectroscopy, J. Electrochem. Soc. 163 (2016) A1373–A1387, https://doi.org/10.1149/2.1141607jes.
[39] R. Raccichini, L. Furness, J.W. Dibden, J.R. Owen, N. García-Araez, Impedance characterization of the transport properties of electrolytes contained within porous electrodes and separators useful for Li-S batteries, J. Electrochem. Soc. 165 (2018) A2741–A2749, https://doi.org/10.1149/2.0631811jes.
[40] M.J. Martínez, S. Shimpalee, J.W. Van Zee, Measurement of macmullin numbers for PEMFC gas-diffusion media, J. Electrochem. Soc. 156 (B80) (2009), https://doi.org/10.1149/1.3005564/XML.
[41] L. Hoffmann, M. Kasper, M. Kahn, G. Gramse, G.V. Silva, C. Herrmann, M. Kurrat, F. Kienberger, High-potential test for quality control of separator defects in battery cell production, Batteries 7 (2021), https://doi.org/10.3390/batteries7040064.